‘Pincer’ Pyridine–Dicarbene–Iridium and -Ruthenium Complexes and Derivatives Thereof

Andreas A. Danopoulos,*[a] Pierre Braunstein,*[b] Jörg Saßmannshausen[c] David C. Pugh[d] and Joseph A. Wright[e]

[a] Professor A. A. Danopoulos
Inorganic Chemistry Laboratory, Department of Chemistry
National and Kapodistrian University of Athens
Panepistimiopolis Zografou, 15771, Athens, Greece
E-mail: A.Danopoulos@chem.uoa.gr
[b] Professor P. Braunstein
CNRS, Chimie UMR 7177, Laboratoire de Chimie de Coordination
Université de Strasbourg
4 rue Blaise Pascal, 67081 Strasbourg Cedex, France
E-mail: braunstein@unistra.fr.
[c] Dr J. Saßmannshausen
Guy's and St Thomas' NHS Foundation Trust and King's College London
16th Floor Tower Wing, Guy’s Hospital, London, SE1 9RT, UK
[d] Dr D. Pugh
Department of Chemistry
King's College London
Britannia House, 7 Trinity Street, London, SE1 1DB, UK
[e] Dr J. A. Wright
Energy Materials Laboratory
School of Chemistry, University of East Anglia,
Norwich Research Park, Norwich, NR4 7TJ, UK

ORCIDs from the authors for this article are available: A. A. D. ORCID 0000-0002-6037-1431; P.B. ORCID 0000-0002-4377-604X; J. S. 0000-0002-4733-5540; D.P. 0000-0001-9600-4708; J.A.W. 0000-0001-9603-1001

Supporting information for this article is given via a link at the end of the document.

Abstract: The cationic pincer-type complexes [Ir^{I}(CN^{Me}C)L]X (CN^{Me}C = (2,6-bis{2,6-diisopropylphenyl}imidazol-2-ylidene)-3,5-dimethylpyridine, L = CO, X = PF_6 **4**; L = CH_3CN, X = PF_6 **5**; L = pyridine, X = BAr^F_4, Ar^F = 3,5-bis-trifluoromethyl-phenyl **6**), that were obtained from [Ir^{I}(CN^{Me}C)Cl] (**1**) by displacement of the chloride ligand were structurally characterized. Complexes **4** and **5** adopt square planar, in-plane distorted geometries, and in **6** the metal environment shows substantial pyramidalization. Theoretical calculations of the cations in **4** and **6** reproduce the experimental structures and rationalize their features. **1** undergoes oxidative transformations with CH_2Cl_2 to *cis*-[Ir^{III}(CN^{Me}C)(CH_2Cl)Cl_2] (**7**) and with $PhICl_2$ to *mer*-[Ir^{III}(CN^{Me}C)Cl_3] (**8**). The ruthenium derivatives *trans*-[Ru^{II}(CNC)Cl_2L] (CNC = (2,6-bis{2,6-diisopropylphenyl}imidazol-2-ylidene)-pyridine, L = pyridine, **10**) and [Ru^{II}(CNC)(η^2,η^2-nbd)L](X)$_2$ (nbd = 2,5-norbornadiene, L = CH_3CN, X = BF_4 **11**), were prepared by the reaction of *cis-trans*-[$RuCl_2$(nbd)$(py)_2$] and *trans-cis*-[$RuCl_2$(nbd)$(pip)_2$] (pip = piperidine) with the ligand CNC, respectively; both adopt distorted octahedral structures. The back-bonding in **11** is comparable to that in its precursor complex, indicating minimal contribution of the NHC donors to this effect. Substitution of both chlorides in the known *cis*-[Ru^{II}(CNC)Cl_2L] (L = PPh_3) by azido ligands gave *cis*-[Ru^{II}(CNC)$(N_3)_2$L] (L = PPh_3, **12**), which by photolytic cleavage of the coordinated N_3 failed to produce well-defined complexes.

Introduction

Although complexes with pincer architectures and N-heterocyclic carbene donors (almost exclusively imidazol-2-ylidenes) have appeared early in the development of the NHC coordination chemistry,[1] there is currently growing research interest in the area.[2] Topical fields amongst others include the extension of the ‘pincer concept’ to other types of NHC donors,[3] the development of non-symmetrical architectures,[4] the study of the pincer non-innocence in the context of metal-ligand cooperation,[5] and the rational incorporation of diverse heteroatoms in the bridgehead and wingtips.[6] Catalytic applications in e.g. hydrogenation, hydrosilylation, electro- and photo-catalytic reduction of CO_2,[7] *ad hoc* catalyst optimization and materials properties are directions also pursued.[7b, 8]

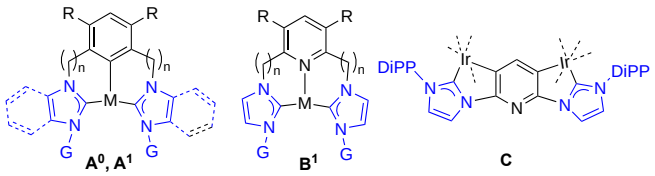

A^0, **B^0** n = 0; **A^1**, **B^1** n=1; R = H, Me; G = aryl or alkyl

Figure 1. Common NHC-containing pincer complexes.

By far the most studied NHC-containing pincer complexes (Figure 1) comprise *m*-phenyl/*m*-xylyl (**A⁰**, **A¹** n = 0, 1, respectively) or pyridine or lutidine (**B⁰**, **B¹** n = 0, 1, respectively) bridgehead moieties; such complexes are known for the majority of transition metals, mainly the late and noble.

In particular, Ir^{III} complexes of type **A⁰** [9] and the related benzimidazol-2-lidenes[10] have been prepared by a range of synthetic methods which reside on the facile metalation of the corresponding bis(imidazolium) salts and of the aromatic C-H bond by an Ir^{I} precursor, (*viz.* $[Ir(\mu\text{-}Cl)(cod)]_2$), in the presence of an external, often weak base (NEt_3 or Cs_2CO_3);[11] the nature of the isolated organometallic product(s) is critically dependent on the type and quantity of the base used. One Ir^{III} analogue of **A¹** is also known.[12]

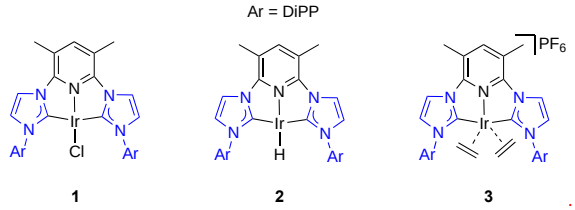

Figure 2. Rare examples of iridium complexes of type **B⁰**.

In contrast, iridium complexes of type **B⁰** are very rare, represented only by **1**, featuring the Ir^{I}-Cl moiety, and its hydride **2** and ethylene **3** derivatives (Figure 2).[13] The difficulty in accessing $Ir^{I/III}$ complexes of type **B⁰** was attributed to the propensity of the Ir-NHC moiety to cyclometallate the pyridine ring, leading to (dinuclear) chelates of type **C** rather than pincers. Consequently, in **1** cyclometallation was blocked by pyridine ring substitution (R = Me, Figures 1 and 2). One Ir^{III} complex with a compartmentalized 'macrocyclic pincer' related to **B¹** (R = H) was recently described.[14]

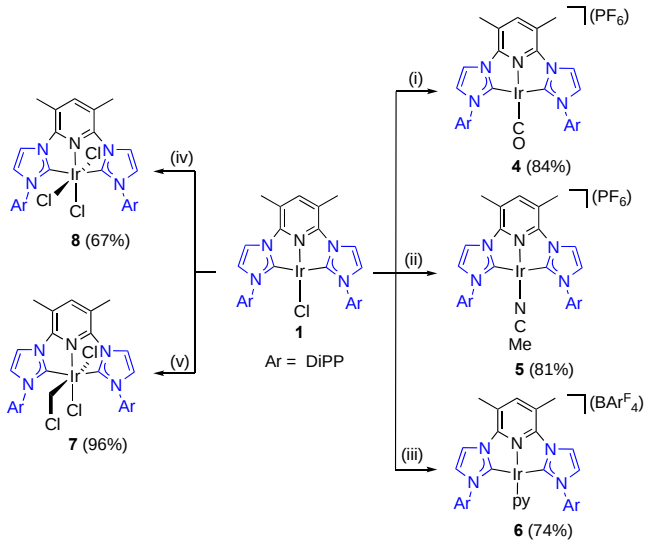

Scheme 1. Ir^{I} and Ir^{III} derivatives originating from **1**. Reagents and conditions: (i) KPF_6, CO, THF, RT; (ii) KPF_6, MeCN; (iii) $NaBAr_4^F$ in pyridine;[13] (iv) CH_2Cl_2; (v) $C_6H_5ICl_2$ in THF.

The Ru complexes of type **B⁰** are comparatively more abundant, and have recently attracted attention as catalysts in the reduction of CO_2; the most promising candidates feature a combination of the pincer ligand with MeCN or chelating bipy co-ligands and *p*-substitution of the bridgehead pyridine heterocycle.[15]

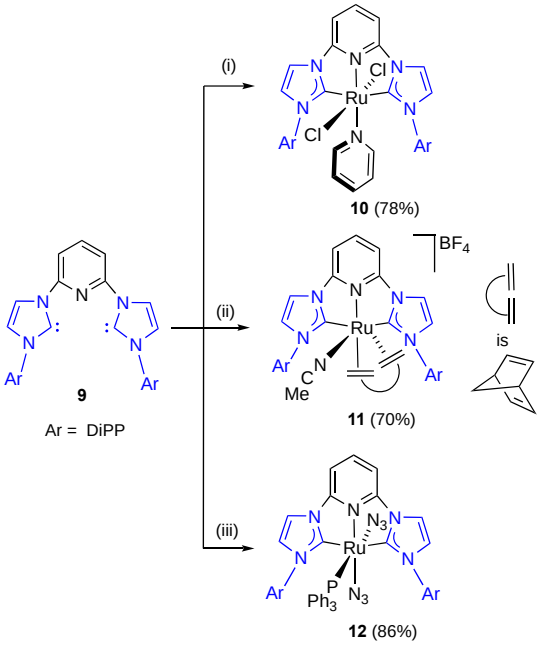

Scheme 2. Ru^{II} pincer complexes prepared from bis(imidazol-2-ylidene)-pyridine (**9**). Reagents and conditions: (i) $[RuCl_2(nbd)(py)_2]$ in THF; (ii) $[RuCl_2(nbd)(pip)_2]$ in THF followed by $AgBF_4$ in CH_3CN; (iii) $[RuCl_2(PPh_3)_3]$ followed by equiv. NaN_3 in THF or $[Ru(CNC)Cl_2(PPh_3)]$ followed by equiv. NaN_3 in THF.

In this paper we describe in detail some derivatives originating from **1** by Cl substitution or metal oxidation. The species **4** – **6** were briefly mentioned previously but no experimental and characterization details were given.[13] We also include three new Ru pincer complexes with a bis(imidazol-2-ylidene)-pyridine-type ligand which expand the limited group of well-defined ruthenium complexes of this type. The electronic structures of **4** and **6** were studied by DFT calculations. A summary of the complexes described herein and the synthetic transformations leading to them are given in Schemes 1 and 2.

Results and Discussion

Ir^{I} Complexes. Complex **4** was obtained as briefly described previously.[13] However, more detailed observations showed that the bubbling of CO through a THF solution of **1** and KPF_6 resulted in a rapid colour change from green to brown, which upon stirring under N_2 for 15 min, turned purple and on re-admission of CO reverted to the original brown; the changes were reversible depending on the concentration of CO. All attempts at characterizing or isolating the brown product were unsuccessful, however, after work up the purple product **4** was obtained as analytically pure solid and characterized spectroscopically.[13] The NMR spectroscopic data are in line with a square planar mono-carbonyl complex with signals at δ 193.08 (Ir-*C*O) and δ 189.69

(Ir-C^{NHC}). The value for the stretching vibration for the coordinated CO (1983 cm^{-1}) is unexpectedly higher than that in the related pincer complex [Ir(PNP)(CO)]PF_6 (PNP = bis(*t*Bu_2Pmethyl)pyridine), (1962 cm^{-1}).[16] A similar trend was described for analogous Fe^0 complexes and rationalized by DFT calculations.[17] A comparative study aiming at understanding the spectroscopic trends in pincer carbonyl complexes as a function of the metal centre and the donor environments will be the subject of a forthcoming publication.[18]

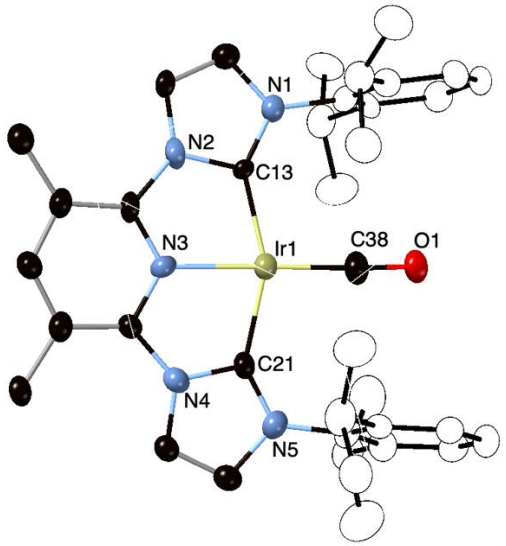

Figure 3. Thermal ellipsoid model of the cation in **4**. Ellipsoids are at 50% probability; H atoms are omitted for clarity. Selected bond lengths [Å] and angles [deg]: C13-Ir1 1.982(8), C21-Ir1 2.017(9), N3-Ir1 2.033(7), C38-Ir1 1.810(8), C38-O1 1.178(10); C38-Ir1-C13 103.3(4), C38-Ir1-C21 101.4(4), C13-Ir1-C21 155.3(3), C38-Ir1-N3 178.8(4), C13-Ir1-N3 77.9(3), C21-Ir1-N3 77.4(3), O1-C38-Ir1 177.1(9).

The solid state structure of **4** has now been confirmed by a X-ray diffraction and is depicted in Figure 3, with selected metrical data in the caption of the Figure. Complex **4** adopts a distorted square planar geometry; prominent distortions from the ideal geometry are due to ligand constraints (*e.g.* angles at Ir: C13-Ir1-N3 77.9(3), C21-Ir1-N3 77.4(3)°).

The Ir–C^{NHC} separations fall in the range of bonding distances.[9b,13] The C–O bond length (1.178(10) Å) is *ca.* 0.05 Å longer than in free CO (1.128 Å) which implies some degree of back-bonding from the Ir^{I}. Despite considering as reasonable the assumption that the initial brown product could be a labile 5-coordinate [Ir^{I}(CN^{Me}C)$(CO)_2$]$^+$, computational studies (discussed below) showed the latter to be more stable than **4** and therefore should be isolable. This discrepancy may have its origin in entropic factors.

Similarly the complex [Ir^{I}(CN^{Me}C)(NCMe)]PF_6 (**5**) that was obtained as a light green powder, was characterized crystallographically after growing single crystals by diffusion of ether into an acetonitrile solution. A model of the cation in **5** is given in Figure 4, with selected metrical data in the caption of the Figure.

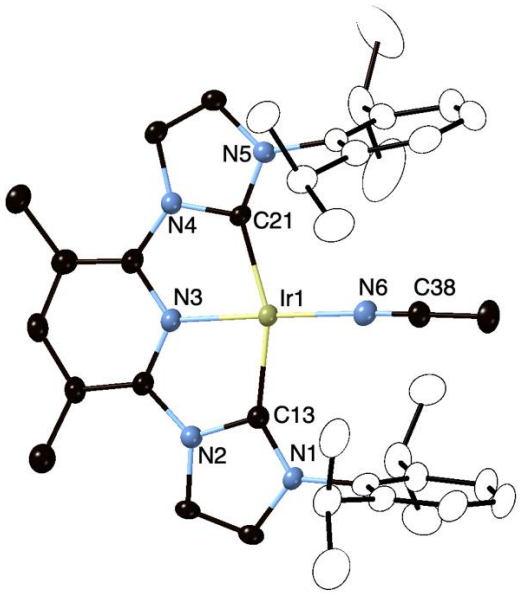

Figure 4. Thermal ellipsoid model (at 50% probability) of one of the four independent cations in the structure of **5**·0.5O$(C_2H_5)_2$; the other three cations have very similar metrical data. Ellipsoids are at 50% probability; H atoms are omitted for clarity. Selected bond lengths [Å] and angles [deg]: C13-Ir1 1.975(6), C21-Ir1 1.990(6), N3-Ir1 1.968(5), N6-Ir1 1.980(5); C21-Ir1-C13 158.1(2), N3-Ir1-N6 178.3(2), N3-Ir1-C13 79.5(2), N3-Ir1-C21 78.6(2), C13-Ir1-N6 99.4(2), C21-Ir1-N6 102.5(2).

A detailed study was undertaken with the complex [Ir^{I}(CN^{Me}C)Py][BAr_4^F] (**6**) that was obtained by the substitution of the chloride in **1** with pyridine and anion exchange with [BAr^F_4]$^-$.REF The ^{1}H-NMR spectrum of **6** is in accord with a structure having only one plane of symmetry (perpendicular to the coordination plane); this concurred with the presence of one signal assignable to C^{NHC} in the $^{13}C\{^1H\}$-NMR spectrum and another for the methyl groups attached to the pyridine bridgehead. However, the total number of aromatic signals in the spectrum pointed to the absence of a second symmetry plane that would coincide with the metal coordination plane. The structure in the solid state was revealed crystallographically and is shown in Figures 5. The cation complex shows a four-coordinate geometry featuring the pincer ligand and one pyridine moiety occupying the fourth coordination site. Importantly, the pyridine ring is 'sandwiched' between the two virtually parallel aromatic rings of the DiPP wingtips and shifted vertically and parallel to the DiPP rings; this distortion may cause the desymmetrization inferred in the NMR spectra. The shift of the pyridine ring imposes a distortion of the square planar geometry and pyramidalization; as a result, the Ir is positioned 0.146 Å above the plane defined by the pincer donors and 0.310 Å above the mean backbone pyridine plane. The separation of the centroids of the DiPP and pyridine rings is *ca.* 3.74 and 3.86 Å. Interestingly, despite the distortion, the metrical data involving the pincer donors are identical within the measured e.s.d. to those of the distortionless **5**.

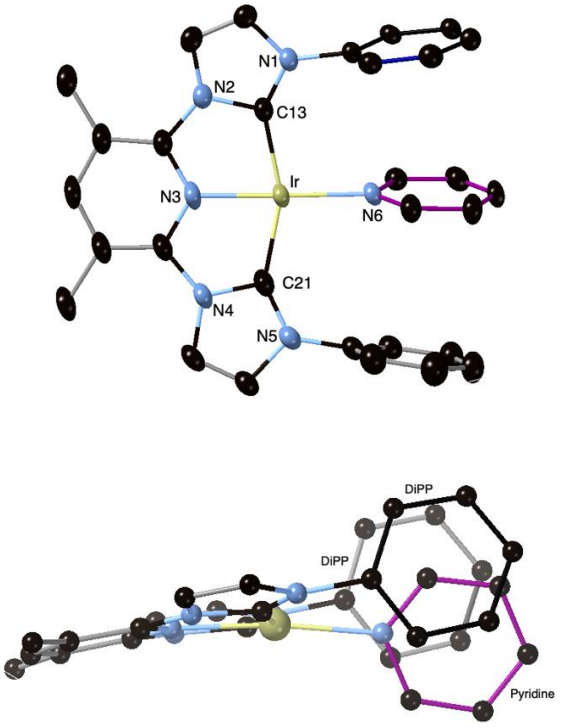

Figure 5. Thermal ellipsoid model (at 50% probability) of the cation in **6.** Top: view down the coordination plane; Bottom: view down the stacked aromatic rings. Ellipsoids are at 50% probability; H atoms and *i*Pr substituents of the DiPP rings are omitted for clarity. Selected bond lengths [Å] and angles [deg]: C13-Ir1 1.998(4), C21-Ir1 1.994(4), N3-Ir1 1.973(3), N6-Ir1 2.058(3); C21-Ir1-C13 156.90(16), N3-Ir1-N6 173.3(1),N3-Ir1-C13 79.0(2), N3-Ir1-C21 78.9(2), C13-Ir1-N6 101.3(1), C21-Ir1-N6 101.4(1).

The origins of the observed distortion were traced in (i) crystal packing forces and/or (ii) intramolecular interactions of covalent or non-covalent nature. In the crystal packing diagram, close contacts between the *m*-hydrogen atoms of the pyridine ring and the CF_3 groups of the $BAr^F{}_4$ anion were detected. However, the inferred persistence of the distortion in solution (*vide supra*) triggered the study of **6** by computational methods; the results are discussed below.

Ir^{III} Complexes. Dissolution of **1** in dichloromethane resulted in a rapid (*ca.* 10 min) colour change of the solution from green to yellow. The ^{1}H NMR spectrum of the isolated product after the work-up is consistent with a desymmetrization across the coordination plane, as evidenced by the four doublets and two septets assignable to the *i*Pr groups of the DiPP; however, only one singlet was observed for the bridgehead pyridine methyl protons and one singlet at δ 1.47 was assigned to a methylene group bound to Ir. In the $^{13}C\{^1H\}$ NMR spectrum, signals assignable to the C^{NHC} and CH_2Cl atoms appeared at δ 175.57 and at δ 13.46, respectively. Consistent with this picture is the solid-state structure of the molecule as established crystallographically (Fig. 6) which revealed the presence of the complex [Ir^{III}(CN^{Me}C)Cl$_2$(CH$_2$Cl)] (**7**) with a σ-chloromethyl ligand in a *cis*-dichloro arrangement supported by the pincer. Evidently, **7** was the product of the oxidative addition of Cl-CH_2Cl to the Ir^I centre of **1.** Despite the geometrical distortions due to the bite angle of the pincer, the Ir–C^{NHC} bond distances are shorter than those of Ir–CH_2Cl, falling into the range of previously observed Ir^{III}–C^{NHC} distances. The pyridine exerts a decreased *trans* influence on the chloride compared to that of the chloromethyl moiety (relevant Ir–Cl bond distances: 2.3584(11) and 2.4783(11) Å, respectively).

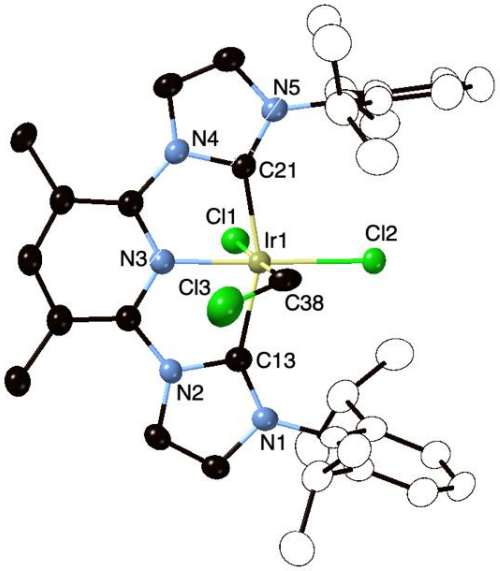

Figure 6. Thermal ellipsoid model (at 50% probability) of **7**. H atoms are omitted for clarity. Selected bond lengths [Å] and angles [deg]: C13-Ir1 2.031(4), C21-Ir1 2.017(4), N3-Ir1 1.979(3), C38-Ir1 2.096(5), Cl1-Ir1 2.478(1), Cl2-Ir1 2.358(1); C21-Ir1-C13 158.3(2), N3-Ir1-Cl2 176.1(1), C38-Ir1-Cl1 176.9(2), C21-Ir1-C38 90.6(2), Cl2-Ir1-Cl1 89.9(4), N3-Ir1-C13 79.3(2).

The oxidative addition of Cl-CH_2Cl to low oxidation state group 9 and 10 complexes is an established reaction albeit with only a handful of structurally characterized products.[19] In the present context, the Rh analogue of **7** has been described[20] and the only two Ir complexes, a pyridine di-imine analogue of **7** and a binuclear species with bridging parent amido (μ-NH_2) groups.[21] Mechanistic details of the reaction have not been studied.

Oxidation of **1** to the yellow Ir^{III} complex [Ir^{III}(CN^{Me}C)Cl$_3$] (**8**) was achieved by using stoichiometric amounts of the chlorine surrogate $PhICl_2$ as oxidant in THF (Scheme 1). The complex was characterized analytically and spectroscopically since crystallization attempts failed. Thus, the ^{1}H NMR spectrum of **8** is consistent with the C_{2v} symmetry of a *mer*-$IrCl_3$ complex: two doublets (δ 1.22 and 1.11) and one septet (δ 3.04) corresponding to the *i*Pr groups of the DiPP wingtips and a singlet at δ 2.95 assignable to the methyl groups on the pyridine ring. The C^{NHC} signal was observed at δ 167.72.

Ru Complexes. In attempts to access new Ru catalyst precursors of type **B^0**, we targeted complexes (neutral or cationic) with labile and/or easily removable co-ligands under catalytic conditions. The recently described cationic butyronitrile and acetonitrile species with 4-G-pyridine-bis(benzimidazol-2-ylidene) and -bis(imidazol-2-ylidene) (G = H,[22] OMe, OH[15c,d]) pincers are the known representatives of this family of complexes; a dozen of bipy-substituted complexes of type **B^0** have been studied as electrocatalysts for the reduction of CO_2.[15b-d,23]

The reaction of the pincer ligand bis(imidazol-2-ylidene)-pyridine **9** with [RuCl$_2$(nbd)(py)$_2$] (2,5-nbd = norbornadiene) in THF

afforded a red solution, from which complex *trans*-[Ru^{II}(CNC)Cl_2(py)] (**10**) was isolated as a red solid. It gave a ^{1}H NMR spectrum consistent with a C_s symmetry *i.e.* two doublets and one septet, which were assigned to the *i*Pr groups of DiPP; the spectrum also demonstrated the retention of one pyridine ligand and the disappearance of the diolefin from the starting material. Thus, in addition to the pincer ligand, the presence of two mutually *trans*-chlorides and one pyridine moieties on the Ru centre were inferred. This was consistent with the $^{13}C\{^1H\}$ NMR spectra and microanalytical data. The lability of the 2,5-norbornadiene in [$RuCl_2$(nbd)$(py)_2$] has been previously observed.[24] The structure of **10** was established crystallographically (Figure 7) and revealed a slightly distorted octahedral coordination geometry. The Ru–C^{NHC} distances fall in the range of previously reported Ru^{II}-NHC complexes. Interestingly, the two Ru–N^{py} bond distances in **10** differ: the Ru-N4 (1.973(5) Å), being part of the pincer is shorter than the Ru-N6 bond (2.120(5) Å) *trans* to it on the monodentate pyridine donor, a difference ascribable to the geometrical constraints imposed by the pincer ligand. The heterocycle of the monodentate pyridine stacks in a parallel face-to-face manner between the aromatic DiPP aromatic rings (*ca.* 3.91 and 3.96 Å between centroids) implying that no stereoelectronic interactions with structural consequences are operating within the aperture created by the latter.

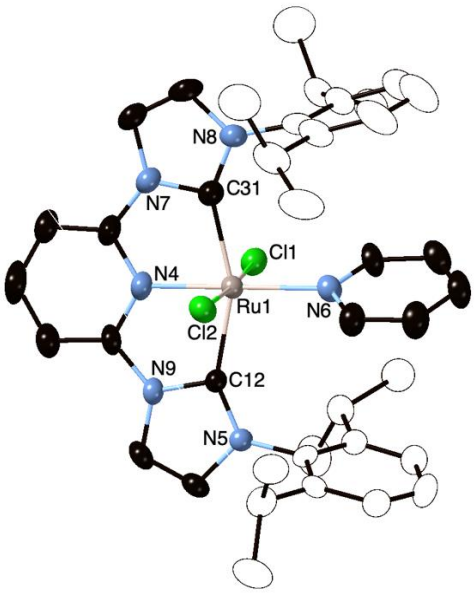

Figure 7. Thermal ellipsoid model (at 50% probability) of **10**; H atoms are omitted for clarity. Selected bond lengths [Å] and angles [deg]: Ru1-C12 2.049(6), Ru1-C31 2.043(5), N4-Ru1 1.973(5), N6-Ru1 2.120(5), Ru1-Cl1 2.444(2), Ru1-Cl2 2.418(2); C31-Ru1-C12 157.2(2), N4-Ru1-N6 179.5(2), Cl2-Ru1-Cl1 175.64(5), N6-Ru1-Cl2 91.76(13), C31-Ru1-Cl1 89.12(15), N4-Ru1-C12 78.3(2).

The substitution of nbd in the complex *trans-cis*-[$RuCl_2$(nbd)(pip)$_2$] (pip = piperidine) is slower than in *trans-cis*-[$RuCl_2$(nbd)$(py)_2$].[24] Consequently, the reaction of the former with **9** proceeded slowly in THF as judged by the minor color change to yellow-orange and the formation of a precipitate. However, the product from this transformation could not be directly characterized; instead exchange of the chlorides by the reaction with $AgBF_4$ in acetonitrile afforded [Ru^{II}(CNC)(nbd)$(NCCH_3)$]BF_4 (**11**) in moderate yields as fine microcrystals after work-up. Although meaningful ^{1}H-NMR spectra were observed, they suffered from relatively broad peaks. The identity and structure of **11** were established by single crystal X-ray diffraction (synchrotron source) (Figure 8). The metal adopted a distorted octahedral coordination geometry (assuming the nbd as bidentate from the middle of the C=C vectors) featuring one pincer, one acetonitrile and one nbd ligands. As anticipated, the distortion is more prominent at the coordination angles subtended by the bonds with the pincer donor atoms. The coordination of the nbd is symmetrical with all four Ru1–C^{alkene} bond distances confined within a narrow range (2.226(2)-2.231(2) Å). The same applies to the alkene bond distances, which are equal within the measured e.s.d.s and slightly elongated compared to the free nbd (1.387(4) Å, 1.391(4) Å and 1.336(3) Å, respectively). For comparison, the nbd bond length in *trans,cis*-[$RuCl_2$(nbd)$(py)_2$] is 1.390 Å[25] and, surprisingly, in [Ru(PCP)(nbd)Cl] (PCP = 1,3-bis (di*iso*propylphosphinomethyl)-phenylene), is *ca.* 1.411 Å,[26] implying again better back-bonding from the metal fragment to the norbornadiene in the latter.

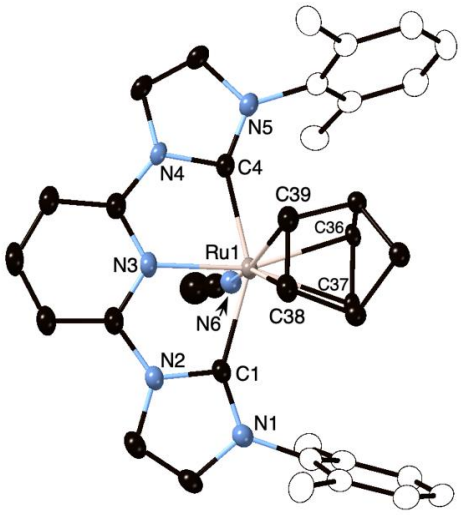

Figure 8. Thermal ellipsoid model (at 50% probability) of the dication in the structure of **11**·2$NCCH_3$. H atoms and the methyls of the *i*Pr in the DiPP wingtips are omitted for clarity. Selected bond lengths [Å] and angles [deg]: N3-Ru1 2.067(2), N6-Ru1 2.074(2), C1-Ru1 2.134(3), C4-Ru1 2.128(3), C36-Ru1 2.205(2), C37-Ru1 2.205(2), C38-Ru1 2.226(2), C39-Ru1 2.231(2), C36-C37 1.391(4), C38- C39 1.387(4), C4-Ru1-C1 151.26(10), N3-Ru1-N6 87.47(8), N3-Ru1-C4 76.24(9), N3-Ru1-C1 75.77(9); N3-Ru1-C36 160.17(9), N3-Ru1-C37 160.0(1), N3-Ru1-C38 102.9(1), N3-Ru1-C39 102.96(9).

Finally, in efforts to access higher oxidation state pincer complexes of ruthenium stabilized by multiple bonded ligands (imido, nitride, *etc.*), we prepared complex *cis*-[Ru^{II}(CNC)$(N_3)_2$$(PPh_3)$] (**12**) by direct exchange of the chlorides in *cis*-[Ru(CNC)$Cl_2$$(PPh_3)$][27] with two equivalents of NaN_3 in THF. Complex **12** was obtained as analytically pure red solid and characterized spectroscopically. An X-ray crystallographic study gave a model for the molecule (Figure 9). Irradiation of **12** in THF led to intractable mixtures.

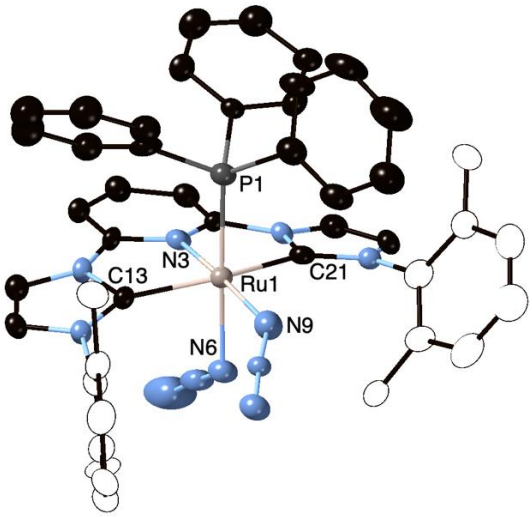

Figure 9. Model of **12**. H atoms and the methyl groups of the *i*Pr in the DiPP wingtips are omitted for clarity. Selected bond lengths [Å] and angles [deg]: C13-Ru1 2.048(5), C21-Ru 2.063(6), N3-Ru1 1.982(4), N6-Ru1 2.165(4), N9-Ru1 2.107(4); Ru1-P1 2.310(1), C21-Ru1-C13 155.3(2), N3-Ru1-N9 174.8(2); N6-Ru1-P1 176.7(2), C21-Ru1-N6 84.3(2), N9-Ru1-P1 93.84(13), N3-Ru1-C13 78.7(2).

DFT calculations

Geometry optimization of 4-dft and 6-dft. Starting from the solid-state structures of **4** and **6**, the structures of the cationic Ir complexes were optimized at the PBE0-D3 level of theory. The inclusion of Grimme's dispersion correction is necessary in order to address any effects of weak interactions like π-stacking or H-bonding.[28] Perusal of the metrical data in **4** *vs*. **4-dft** and **6** *vs*. **6-dft** revealed a good agreement between the calculated and observed values. Deviations were only noticed in the *i*Pr substituents of the DiPP, which can be attributed to crystal packing effects. Relevant metrical data for **4** vs. **4-dft** and **6** vs. **6-dft** are compared in Tables 1 and 2, respectively. Overall, from the comparison it appears that the calculated structures show a higher symmetry. Crystal packing effects should affect the experimental structure, which were not included in the calculations.

The hypothesis that the reversible colorations in the preparation of **4**, which depended on the excess of CO present, were due to the transient formation of a complex $[Ir(CN^{Me}C)(CO)_2]^+$ (*vide supra*) was further scrutinized by computing the postulated bis-carbonyl structure **13-dft**. Relevant metrics are shown in Table 3.

Table 1. Comparison of metrical data in the observed and the calculated structure of the cations in **4** and **4-dft**. Distances are in Å, angles in degrees.

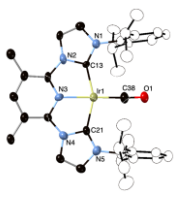

4*

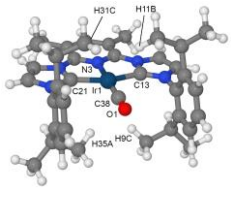

4-dft

Ir1-C13	1.982(8)	2.005
Ir1-C21	2.017(9)	2.005
Ir1-N3	2.033(7)	2.054
Ir1-C38	1.810(8)	1.856
C38-O1	1.178(10)	1.144
Ir1-H9C	3.317	2.993
Ir1-H11B	3.144	2.992
Ir1-H31C	3.271	2.992
Ir1-H35A	3.849	2.992
N3-Ir1-C38	178.8(4)	180.00
C13-Ir1-C21	155.3(3)	156.31
Ir1-C38-O1	177.1(9)	180.00

[*] The atoms H9C, H11B, H31C and H35A are not shown in the picture

Table 2. Comparison of metrical data in the observed and the calculated structure of the cations in **6** and **6-dft**. Distances are in Å, angles in degrees.

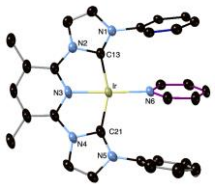

6*

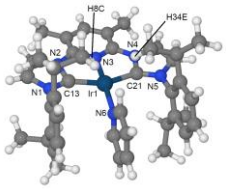

6-dft

C13-Ir1	1.975(6)	1.999
Ir1-C21	1.990(6)	1.999
N3-Ir1	1.968(5)	1.987
Ir1-N6	1.980(5)	2.069
H34E-Ir1	3.285	2.950
H8C-Ir1	3.103	2.949
N3-Ir1-N69	178.3(2)	174.88
C13-Ir1-C21	158.1(2)	156.67

[*] The atoms H8C and H34E are not shown in the picture

Table 3. Metrical data of the calculated structure **13-dft**. Distances are in Å, angles in degrees

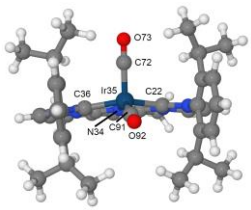

13-dft

C22-Ir35	2.019	C22-Ir35-C36	150.96
Ir35-C36	2.019	N34-Ir35-C91	148.00
N34-Ir35	2.063	C22-Ir35-C72	99.30
Ir35-C91	1.888	Ir35-C91-O92	175.49
Ir35-C72	1.924	Ir35-C72-O73	174.20
C91-O92	1.143		
C72-O73	1.141		

Unlike in **4** and **4-dft**, the iridium in **13-dft** is in a square pyramidal environment with one apical and one basal CO and is located above the basal plane. This geometry led to slight variation of the bond distances between the corresponding donors and the iridium in **4-dft** and **13-dft**; in addition, the apical Ir-CO bond is slightly longer than the basal Ir-CO one. In order to estimate the relative stabilities of **4-dft** and **13-dft**, *i.e.* to evaluate the extent of the equilibrium shown in Scheme 3, a simple energy and free energy calculation of both products and CO was performed. It was found that **13-dft** is slightly more stable in the gas phase by -79.48 kJ/mol (free energy: -26.60 kJ/mol).

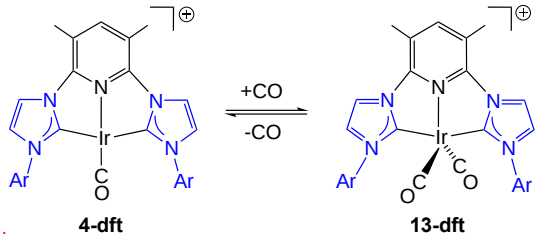

Scheme 3. Postulated equilibrium between **4-dft** and **13-dft**

This unexpected result warrants some further explanation. Although the calculated data point to the equilibrium lying on the side of **13-dft**, we only obtained **4** experimentally. Assuming that the association/dissociation of the CO is nearly barrierless, it is tempting to assume that excluding the CO from the equilibrium will shift it to the left-hand side of the equation and thus lead to the formation of **4-dft** exclusively.

Electronic properties of 4-dft, 6-dft, and 13-dft. In order to obtain further insight into the electronic properties, in particular with relation to the origin of the unusual deformation of **6** and **6-dft**, we followed the usual approach of combining QTAIM with the NBO, as it provides a good understanding of the nature of the bonds. These tools were complemented by a Non-covalent Interaction (NCI) calculation, which captures more subtle interactions such as hydrogen - element or π-stacking interactions. Full details, in particular the interactions obtained from NBO calculations, are given in ESI.

Table 4. Electron density and Laplacian plot of **4-dft**: plot along the NHC ligand plane.

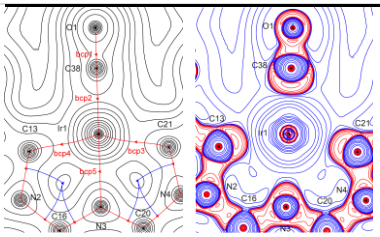

	ρ(*r*)	$\nabla^2\rho(r)$
bcp1	0.4680	-0.1328
bcp2	0.1855	-0.1095
bcp3	0.1499	-0.0566
bcp4	0.1499	-0.0566
bcp5	0.1165	-0.1026

From the negative Laplacians of the bond critical points, we concluded that the interactions between Ir and C13, C21 and C38 are of open shell, *i.e.* ionic character, as expected.

Attempts were undertaken to compare the stability of **13-dft** with respect to the loss of CO with that of the previously reported (d^8) [Fe($CN^{Me}C$)$(CO)_2$]. The differences are shown in Tables 5 and 6, respectively.[17]

Table 5. QTAIM result of **13-dft** structure

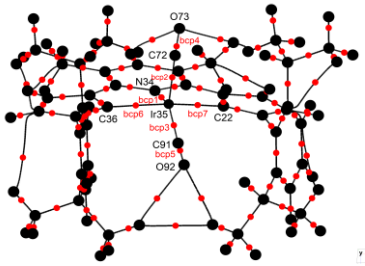

	ρ(r)	$\nabla^2\rho(r)$
bcp1	0.1205	-0.09208
bcp2	0.1655	-0.08453
bcp3	0.1768	-0.09000
bcp4	0.4705	-0.14899
bcp5	0.4682	-0.13851
bcp6	0.1475	-0.04767
bcp7	0.1475	-0.04767

Table 6. QTAIM results of [Fe(CNMeC)$(CO)_2$][17]

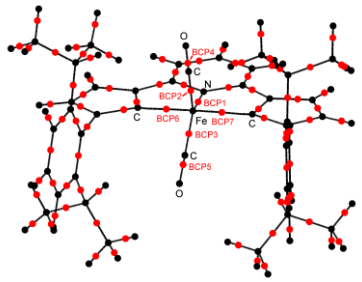

]	ρ(*r*)	$\nabla^2\rho(r)$]
BCP1	0.1044	-0.13848
BCP2	0.1600	-0.14209
BCP3	0.1530	-0.14470
BCP4	0.4386	-0.24520
BCP5	0.4392	-0.24421
BCP6	0.1134	-0.08684
BCP7	0.1134	-0.08684

For example, the difference between the M-C(O) bond critical points bcp2 and bcp3, which correspond to the M-$(CO)_{apical}$ and the M-$(CO)_{basal}$ bonds, respectively, is higher for **13-dft** compared to the Fe complex (0.0113 *vs.* 0.0070). Furthermore, in **13-dft**, bcp2 has a lower electron density compared with bcp3 whereas in the Fe complex the situation is reversed, *i.e.* bcp2 has the higher electron density relative to bcp3. Thus, it can be concluded that in **13-dft** the CO_{apical} is more weakly bound than in the Fe complex where these bonds appear to be very similar. This fact is also mirrored in the longer bond distance between Ir-$(CO)_{apical}$ (2.019 Å) compared with Ir-$(CO)_{basal}$ (1.888Å). These points may explain the difficulty in experimentally isolating **13-dft** which is contrasted to the stability of the Fe complex.

An additional feature identified in both **4-dft** and **6-dft** is a weak interaction between some of the *i*Pr hydrogens of the DiPP wingtip and iridium. As the QTAIM analysis clearly showed a bond path connecting the H with the iridium, it is tempting to speculate about the presence of an agostic interaction between them. Given the rather long distance between the atoms involved (ca. 2.992 Å), we expected it to be weak. Table 7 shows one of these interactions found in one half of the molecule; the other half exhibits a similar behaviour.

Table 7. Electron density and Laplacian plot of **6-dft** along the Ir-H plane. Only one of the two pairs of the H interactions is shown.

	ρ(r)	$\nabla^2\rho(r)$
bcp1	0.0055	-0.0040
bcp2	0.0096	-0.0055

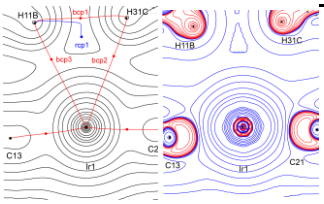	bcp3	0.0096	-0.0055

In order to obtain insight into the nature of these interactions, in particular to establish if they are agostic, we performed a NBO analysis. The results are summarised in Table 8.

Table 8. NBO analysis of **4-dft**; only one set of the Ir-H interactions is shown.

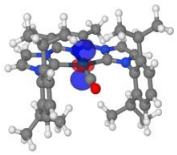	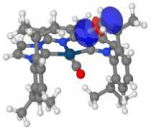	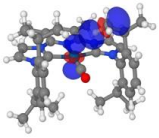
mo82	mo219	mo82 → mo219 E_{2P} = 1.01 kcal/mol
Ir($sd^{8.77}$)	C($sp^{3.17}$)-H(s)	

The results clearly show an interaction of a filled Ir orbital of predominantly d-character ($sd^{8.77}$) with the *antibonding* C-H orbital. This is the reverse situation of an *agostic* bond, where the *filled* C-H bond is donating electron density into an *empty* metal orbital of suitable symmetry.[29] As these interactions are weak, they will probably be easily affected by solvent or crystal packing effects. Nevertheless, the NCI analysis validates their presence.[30]

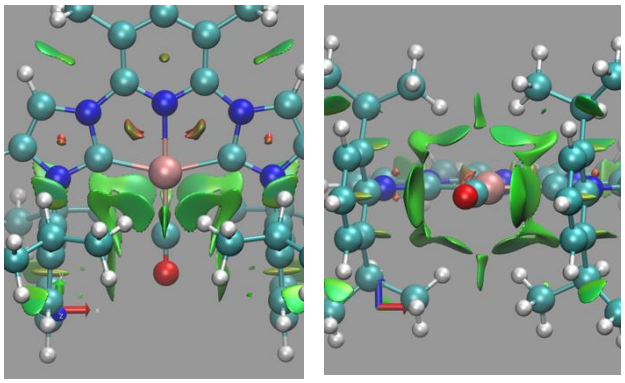

Figure 10. NCI analysis of **4-dft**. Left: View from above the coordination plane; Right: View along the coordination plane.

The visualization of non-covalent interactions (NCIs) is based on the analysis of the reduced density gradient at low densities, *i.e.* the tail end of the electron density between to atoms is analysed. In this way, weak interactions between atoms are picked up, *e.g.* the interaction between the benzene dimer in the parallel offset stacking mode. The two views in Figure 10 use the usual colour code (blue for highly attractive hydrogen bonding interactions, red for steric repulsion and green for very weak interactions of the van der Waals or dipolar type). In Figure 10(left) the green surface between the H and the Ir provides supporting evidence for the interaction between the H atoms of the *i*Pr and the Ir by the NCI analysis; in Figure 10(right) the dipole-dipole interactions between the O and the centre of the aromatic rings are visible.

The geometrical distortion observed experimentally in **6** was also reproduced in **6-dft**. It is therefore reasonable to assume that crystal packing effects cannot be solely responsible for the distortion (see also above) but that other intramolecular forces should be at play. A QTAIM analysis of **6-dft** did not reveal anything unusual. The electron density at the bond critical point between the pincer nitrogen and Ir is 0.1350 (compared with 0.1165 for **4-dft**); minor differences of this magnitude are expected when the CO ligand is replaced with pyridine. However, NBO analysis revealed an unexpected result (see Table 9).

Table 9. NBO analysis of **6-dft;** only the Ir-N interactions are shown.

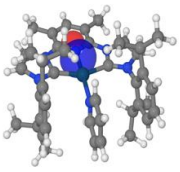	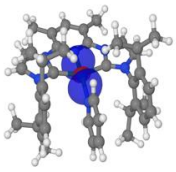	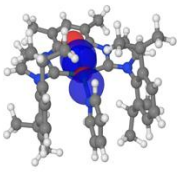
mo84	mo211	mo84→ mo211 E_{2P} = 185.09 kcal/mol
N($sp^{3.64}$)	Ir($sd^{0.72}$)	
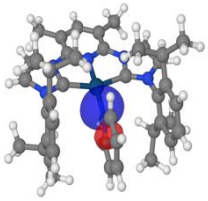	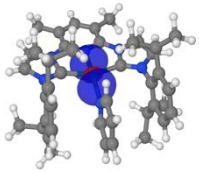	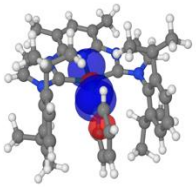
mo91	mo211	mo91 → mo211 E_{2P} = 171.32 kcal/mol
N($sp^{3.46}$)	Ir($sd^{0.72}$)	

The two nitrogen atoms interact with the same empty orbital of iridium and thus compete for this orbital. From the NBO analysis, it can be seen that the second order perturbation energy (E2P) for the pincer-ligand N→Ir interaction is 185.09 kcal/mol, significantly larger than the pyridine N → Ir interaction (only 171.32 kcal/mol). One explanation for this could be the relative freedom of the monodentate pyridine donor to adjust its bonding distance to Ir compared with that of the more rigid pincer-pyridine donor. The position of both DiPP ligands is locked in place due to isopropyl H-Ir interaction (*cf.* **4-dft**), however in **6-dft** only the hydrogen atoms H8C and H34E take part in this interaction. In contrast to **4-dft**, in **6-dft** we find a larger E2P of 1.48 kcal/mol concomitant with a shorter Ir-H distance of 2.950 Å (2.992 Å for **4-dft**). Furthermore, the other isopropyl hydrogen atoms H11A

and H31C interact with the pyridine carbon atoms C38 and C39, although these interactions are very weak (E2P = 0.55 kcal/mol).

Further support for these bonding interactions is obtained from the NCI analysis. Subtle interactions between the pyridine heterocycle and both DiPP wingtips were found. The overall picture is that the pyridine ring is subject to a parallel offset stacking, as illustrated in Figure 11.

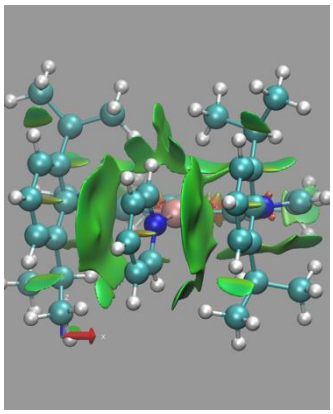

Figure 11. NCI plot of **6-dft**

The interactions among all three aromatic systems are clearly visible; the green area between the rings indicates weak interaction and, from the position of the aromatic rings relative to each other, we conclude that it is mostly a dipole-dipole interaction. The centre of one aromatic ring interacts with the electron cloud of the other.

As mentioned before, these subtle effects, when taken separately, appear of lesser significance. However, *in concerto*, they may lead to observable structural outcomes. We conclude that the interaction (electron donation) of both N atoms with the same empty Ir orbital leads to an Ir-N bond weakening situation. Under the effect of π-stacking and Ir → H interactions, the molecule relaxes by moving the monodentate pyridine out of the coordination plane, thus maximizing these interactions and minimizing its overall energy. Consequently, the distortion observed both in the solid-state and the calculated structures can be mainly attributed to intramolecular interactions.

Conclusion

The rare pincer dicarbene complex [Ir^{I}(CN^{Me}C)Cl] served as an entry point to the synthesis of new derivatives by chloride substitution or metal oxidation, thus expanding the small group of Ir compounds of this type. There are few interesting features emerging from the present study: (i) the importance of suppressing pyridine cyclometallation; (ii) the facile oxidative reactivity of the Ir in this environment; (iii) the involvement of subtle intramolecular interactions, also of non-covalent nature, which synergistically work to observable structural effects. On the other hand, details of the understanding of the electronic structure of the CNC complexes require further refinement. In particular, insight will be gained by the comparison with CNC complexes of Ru (*cf*. **11** – **12** above and related), Os and other metals, and complexes with alternative pincer designs bearing classical (PNP) or mixed classical and NHC (PNC) donors. This objective, as well as the accessibility of synthetic targets with applications in catalysis and photophysics based on the high reactivity of the [Ir^{I}(CN^{Me}C)Cl complex and the new derivatives described herein are under way in our laboratories.

Experimental Section

Experimental Details

General considerations. All manipulations involving metal amides were performed under nitrogen or argon in a MBraun glove-box. Solvents (THF, ether) were dried using standard methods and distilled under nitrogen prior to use or passed through columns of activated alumina and subsequently purged with nitrogen or argon (toluene, pentane). After drying, the solvents were stored over K mirror in the glove box until use. The starting materials were prepared according to literature procedures: **1**,[13] **9**,[31] *trans*,*cis*-[$RuCl_2$(nbd)(py)$_2$], [$RuCl_2$(nbd)(pip)$_2$][24] (py = pyridine, pip = piperidine, $NaBAr^F{}_4$ Ar^F = 3,5-bis-trifluoromethyl-phenyl).[32] The complexes **4**, **5** and **6** were prepared as described previously;[13] more detailed procedures are given in the ESI. ^{1}H-NMR spectra were recorded on a Bruker AVANCE III spectrometer (400 MHz) at 298 K unless stated otherwise. The ^{13}C{^{1}H} spectra were assigned on the basis of DEPT-135, HMQC and HSBC experiments. Elemental analyses were carried out in the London Metropolitan University.

(2,6-Bis(2,6-di*iso*propylphenyl)imidazol-2-ylidene)-3,5-dimethylpyridine iridium(III) chloromethyl dichloride; Complex **7**

Complex **1** (0.075 g, 0.10 mmol) was dissolved in dry dichloromethane (20 mL) and the solution was stirred for 1 h. After removal of the volatiles under reduced pressure, the solid was crystallised as yellow needles by slow diffusion of ether into a dichloromethane solution. Yield: 0.080 g, *ca*. 96%. Analysis (%): Calc. for $C_{38}H_{47}N_5IrCl_3$: C, 52.32; H, 5.43; N, 8.03. Found: C, 52.44; H, 5.45; N 8.14. NMR (C_6D_6): ^{1}H (400.0 MHz), δ 8.06 (2H, d, *J* = 2.0 Hz, imidazol-2-ylidene), 7.44 (1H, s, py-Me), 7.34–7.26 (4H, m, DiPP), 7.19–7.10 (2H, m, DiPP), 7.02 (2H, d, *J* = 2.0 Hz, imidazol-2-ylidene), 3.29 (2H, septet, *J* = 6.5 Hz, C*H*(CH_3)$_2$), 2.77 (6H, s, py-Me), 2.63 (2H, septet, *J* = 6.5 Hz, C*H*(CH_3)$_2$), 1.47 (2H, s, CH_2Cl), 1.19, 1.13, 1.08, 0.95 (each 6H, d, *J* = 6.5 Hz, CH(CH_3)$_2$). ^{13}C{^{1}H} (100.6 MHz): δ 175.57 (C, C^{NHC}), 152.09, 147.52 (C, Ar), 147.21 (CH, Ar), 145.21, 134.17 (C, Ar), 129.60, 124.90, 123.68, 122.96, 118.94 (CH, Ar), 116.66 (C, Ar), 29.26, 28.07, 26.05, 25.81, 22.93, 22.54 (CH(CH_3)$_2$), 19.29 (CH_3, py-Me), 13.46 (*C*H_2Cl).

(2,6-Bis(2,6-di*iso*propylphenyl)imidazol-2-ylidene)-3,5-dimethylpyridine iridium (III) chloride; Complex **8**

To a solution of complex **1** (0.150 g, 0.19 mmol) in THF (20 mL) was added $PhICl_2$ (0.058 g, 0.19 mmol) under a counterflow of N_2. The yellow solution was stirred for 16 h, filtered and the volatiles were removed under reduced pressure giving a solid residue, which was dissolved in the minimum amount of dichloromethane. A yellow powder was precipitated by slow addition of ether (50 mL). Yield: 0.110 g *ca*. 67%. Analysis (%): Calc. for $C_{37}H_{45}N_5IrCl_3$: C, 51.77; H, 5.28; N 8.16. Found: C 51.71, H 5.23; N 8.10. NMR (C_6D_6): ^{1}H (400.0 MHz), δ 8.68 (1H, s, py-Me), 8.32 (2H, d, *J* = 6.5 Hz, imidazol-2-ylidene), 7.54 (2H, d, *J* = 6.5 Hz, imidazol-2-ylidene), 7.41 (4H, d, *J* = 8.0 Hz, Ar), 7.24 (2H, t, *J* = 8.0 Hz, Ar), 3.04 (4H, septet, *J* = 6.5 Hz, C*H*(CH_3)$_2$), 2.95 (6H, s, py-Me), 1.22, 1.11 (each 12H, d, *J* = 6.5 Hz, CH(CH_3)$_2$). ^{13}C{^{1}H} (100.6 MHz): δ 167.72 (C, C^{NHC}), 153.10 (CH, Ar), 147.25 (C, Ar), 138.29 (CH, Ar), 135.16 (C, Ar), 132.03 (CH, Ar), 128.10 (C, Ar), 127.66, 125.06 (CH, Ar), 120.38 (C, Ar), 28.88 (CH, CH(*C*H_3)$_2$), 26.68, 22.14 (CH(*C*H_3)$_2$), 19.97 (*C*H_3, py-Me) ppm.

(2,6-Bis(2,6-di*iso*propylphenyl)imidazol-2-ylidene)pyridine ruthenium(II) pyridine dichloride; Complex **10**

Trans,*cis*-[$RuCl_2$(nbd)$(py)_2$] (0.300 g, 0.71 mmol) and **9** (0.377 g, 0.71 mmol) were dissolved in THF (30 mL) at room temperature and the solution was stirred for 6 h. Then the solvent was evaporated under reduced pressure, the solid residue was washed with pentane (20 mL) and dried under vacuum. Crystallization was carried out by slow diffusion of diethyl ether into a dichloromethane of the red solid, affording red-brown crystals. Yield: 0.430 g, *ca*. 78%. Analysis: Found (Calcd. for $C_{40}H_{46}N_6Ru$) (%): C, 61.29 (61.37); H, 5.88 (5.92); N, 10.62 (10.74). NMR (CD_2Cl_2): ^{1}H (400.0 MHz), δ 8.42 (2H, dd, *J* = 6.5, 1.5 Hz, Ar), 7.96 (2H, d, *J* = 2.0 Hz, Ar), 7.63–7.52 (2H, m, Ar), 7.41–7.28 (7H, m, Ar), 7.19–7.08 (2H, m, Ar), 7.03 (1H, d, *J* = 2.0 Hz, Ar), 6.94 (2H, d, *J* = 8.0 Hz, Ar), 3.07 (4H, septet, *J* = 7.0 Hz, *i*Pr CH), 0.97, 0.91 (each 12H, d, *J* = 7.0 Hz, *i*Pr CH_3). ^{13}C(^{1}H) (100.6 MHz): δ 204.33 (C, C^{NHC}), 157.96 (C, Ar), 154.98 (CH, Ar), 148.44, 147.67, 136.91 (C, Ar), 134.16, 132.50 (CH, Ar), 130.95 (C, Ar), 130.25 (CH, Ar), 126.48 (C, Ar), 126.37, 125.32, 124.75, 123.91, 121.46, 116.57, 104.16 (CH, Ar), 28.28 (*i*Pr CH), 26.52, 22.90 (CH_3, *i*Pr).

(2,6-Bis(2,6-di*iso*propylphenyl)imidazol-2-ylidene)pyridine-η^2,η^2-2,5-norbornadiene-acetonitrile)-ruthenium(II) bis-(tetrafluoroborate) bis acetonitrile; Complex **11**

To a suspension of [$RuCl_2$(nbd)$(pip)_2$] (0.300 g, 0.69 mmol) in THF (30 mL) at -78 °C was added a solution of **9** (0.368 g, 0.69 mmol) in THF (*ca*. 10 mL), which was immediately allowed to warm to room temperature and stirred for 3 d. Then the volatiles were removed under reduced pressure and the brown residue was dissolved in acetonitrile (*ca.* 40 mL) and $AgBF_4$ (0.272 g, 1.4 mmol) was added as a solid. The resulting suspension was stirred for one day, filtered through Celite and the resultant yellow brown solution was concentrated to *ca*. 10 mL and layered with ether. Dark yellow crystals appeared after 2 d. Yield: 0.485 g, *ca*. 65%. Acceptable combustion analysis data could not be obtained due to the presence of volatile CH_3CN in the crystals (see also crystallographic part). NMR (CD_3CN): ^{1}H (300.0 MHz), δ 8.42–7.90 (5H, m), 7.96 (2H, Ar), 7.25–7.08 (4H, m, Ar), 7.03 (2H, d, *J* = 2.0 Hz, Ar), 7.03 (2H, br, imid), 6.94 (2H, br imid), 4.45 (m, 4H norbornadiene), 2.45 (d, 2H norbornadiene) 2.25 (d, 2H, norbornadiene), 2.0 (*ca*. 6H, br, CH_3CN), 2.85–2.25 (4H, m, *i*Pr CH), 1.28–0.85 (24H, m, *i*Pr CH_3). ^{13}C{^{1}H} (75.5 MHz): δ 202.0 (C, C^{NHC}), 158.9 (C, Ar), 155.2 (CH, Ar), 148.5, 132.0 (CH, Ar), 130.3 (CH, Ar), 126.5 (C, Ar), 126.2, 115.2, 103.1 (CH, Ar), 73.2, 71.5 (CH=CH norb), 51.2 (CH_2 norbn), 62.3 (CH norb), 28.55 (CH, *i*Pr), 25.52, 23.10 (CH_3, *i*Pr).

(2,6-Bis(2,6-diisopropylphenyl)imidazol-2-ylidene)pyridine ruthenium(II) triphenylphosphine diazide; Complex **12**

The complex (2,6-bis(2,6-diisopropylphenyl)imidazol-2-ylidene)pyridine triphenylphosphine ruthenium dichloride (0.188 g, 0.19 mmol) and NaN_3 (0.063 g, 0.97 mmol) were dissolved in THF (20 mL) and the solution was stirred for 16 h. The solvent was then evaporated under reduced pressure, the residue dissolved in dichloromethane and the solution filtered through Celite. Crystallization occurred by slow diffusion of diethyl ether into a dichloromethane solution. Yield: 0.156 g, *ca*. 86%. Analysis: Found (Calcd. for $C_{53}H_{56}N_7PRu$ *i.e.* $C_{53}H_{56}N_{11}PRu - 2N_2$) (%): C, 68.91 (65.01); H, 6.06 (5.76); N, 10.49 (15.74). NMR (CD_2Cl_2): ^{1}H (300.0 MHz), δ 8.25–7.93 (1H, m, Ar), 7.77–6.98 (23H, m, Ar), 6.88–6.76 (4H, m, Ar), 2.82–2.14 (4H, m, *i*Pr CH), 1.34–0.70 (24H, m, *i*Pr CH_3). ^{13}C{^{1}H} (75.5 MHz): δ 157.43, 148.97, 136.20 (C, Ar), 134.14 (CH, d, *J* = 10.0 Hz, *o*-PPh_3), 132.67, 131.12, 130.17, 129.74 (CH, Ar), 129.35 (CH, *p*-PPh_3), 129.22 (C, Ar), 128.70 (CH, Ar), 128.47 (CH, d, *J* = 9.0 Hz, *m*-PPh_3), 125.30, 124.72, 123.77, 116.09, 105.35 (CH, Ar), 26.53, 26.30, 22.48, 22.23 (CH/CH_3, *i*Pr). ^{31}P{^{1}H} (121.5 MHz): δ (121.5 MHz): 151.27.

Density Functional Theory (DFT) Calculations

DFT calculations were conducted using Gaussian09, Rev. D.01.[33] Calculations were performed at the PBE-D3 level of theory.[34] A mixed basis set consisting of Pople's triple zeta 6-311G(d,p) basis set[35] for all elements but for Ir where the Stuttgart-Dresden electron core potential basis set (keyword SDD) was employed. This mixture of basis set is abbreviated ecp11. Analytical frequency calculations were performed for the obtained structure to ensure a minimum on the potential energy surface (no imaginary frequencies). This functional and basis set combination have been shown to be most accurate and reliable for third row transition metal compounds.[36] For the Bader and NBO calculations, the Stuttgart-Dresden basis set was replaced with the all electron basis set SARC-DKH2,[37] obtained from the basis set exchange website,[38] in connection with the relativistic DKH2 approach, as implemented in Gaussian09. Quantum Theory of Atoms in Molecules (QTAIM) analysis[39] were performed with the AIM2000 program.[40] For the Natural Bond Orbital analysis (NBO), the NBO 7.0 program was used.[41] For the Non-Covalent Index calculation the program *nci-plot* was used.[30] Jmol was used for the graphical representation of the molecules.[42]

Acknowledgements

A.A.D acknowledges support by a Special Account for Research Grant (S.A.R.G) for the 'Re-initiation of Research' administered by the Rector of the National and Kapodistrian University of Athens. P. B. thanks the CNRS and he University of Strasbourg for support. J.S. acknowledges access to the research computing facility at King's College London, Rosalind (https://rosalind.kcl.ac.uk), delivered in partnership with the National Institute for Health Research (NIHR) Biomedical Research Centres at South London & Maudsley and Guy's & St. Thomas' NHS Foundation Trusts, and part-funded by capital equipment grants from the Maudsley Charity (award 980) and Guy's & St. Thomas' Charity (TR130505). The views expressed are those of the author(s) and not necessarily those of the NHS, the NIHR, King's College London, or the Department of Health and Social Care.

Keywords: NHC ligands • oxidative-addition • pincer complexes theoretical calculations • iridium • ruthenium

References

[1] (a) A. A. D. Tulloch, A. A. Danopoulos, G. J. Tizzard, S. J. Coles, M. B. Hursthouse, R. S. Hay-Motherwell, W. B. Motherwell, *Chem. Commun.* **2001**, 1270-1271; (b) J. C. C. Chen, I. J. B. Lin, *J. Chem. Soc., Dalton Trans.* **2000**, 839-840; (c) E. Peris, J. A. Loch, J. Mata, R. H. Crabtree, *Chem. Commun.* **2001**, 201-202.

[2] (a) D. Pugh, A. A. Danopoulos, *Coord. Chem. Rev.* **2007**, *251*, 610-641; (b) R. E. Andrew, L. González-Sebastián, A. B. Chaplin, *Dalton Trans.* **2016**, *45*, 1299-1305; (c) K. Farell, M. Albrecht, *Topics in Organomet. Chem.* **2016**, *54*, 45-91.

[3] (a) G. A. Filonenko, E. Cosimi, L. Lefort, M. P. Conley, C. Copéret, M. Lutz, E. J. M. Hensen, E. A. Pidko, *ACS Catalysis* **2014**, *4*, 2667-2671; (b) G. Kleinhans, G. Guisado-Barrios, D. C. Liles, G. Bertrand, D. I. Bezuidenhout, *Chem. Commun.* **2016**, *52*, 3504-3507; (c) G. Kleinhans, M. M. Hansmann, G. Guisado-Barrios, D. C. Liles, G. Bertrand, D. I.

Bezuidenhout, *J. Am. Chem. Soc.* **2016**, *138*, 15873-15876; (d) R. P. Yu, J. M. Darmon, S. P. Semproni, Z. R. Turner, P. J. Chirik, *Organometallics* **2017**, *36*, 4341-4343; (e) H. Wang, B. Zhang, X. Yan, S. Guo, *Dalton Trans.* **2018**, *47*, 528-537.

[4] (a) T. Simler, L. Karmazin, C. Bailly, P. Braunstein, A. A. Danopoulos, *Organometallics* **2016**, *35*, 903-912; (b) D. A. Valyaev, J. Willot, L. P. Mangin, D. Zargarian, N. Lugan, *Dalton Trans.* **2017**, *46*, 10193-10196; (c) S. Gu, J. Du, J. Huang, Y. Guo, L. Yang, W. Xu, W. Chen, *Dalton Trans.* **2017**, *46*, 586-594; (d) D. Yang, J. Dong, B. Wang, *Dalton Trans.* **2018**, *47*, 180-189; (e) D. Kim, L. Le, M. J. Drance, K. H. Jensen, K. Bogdanovski, T. N. Cervarich, M. G. Barnard, N. J. Pudalov, S. M. M. Knapp, A. R. Chianese, *Organometallics* **2016**, *35*, 982-989; (f) P. Sánchez, M. Hernández-Juárez, E. Álvarez, M. Paneque, N. Rendón, A. Suárez, *Dalton Trans.* **2016**, *45*, 16997-17009.

[5] (a) R. P. Yu, J. M. Darmon, C. Milsmann, G. W. Margulieux, S. C. E. Stieber, S. DeBeer, P. J. Chirik, *J. Am. Chem. Soc.* **2013**, *135*, 13168-13184; (b) T. Simler, P. Braunstein, A. A. Danopoulos, *Chem. Commun.* **2016**, *52*, 2717-2720; (c) T. Simler, A. A. Danopoulos, P. Braunstein, *Dalton Trans.* **2017**, *46*, 5955-5964; (d) C. F. Harris, M. B. Bayless, N. P. van Leest, Q. J. Bruch, B. N. Livesay, J. Bacsa, K. I. Hardcastle, M. P. Shores, B. de Bruin, J. D. Soper, *Inorg. Chem.* **2017**, *56*, 12421-12435.

[6] A. Eizawa, S. Nishimura, K. Arashiba, K. Nakajima, Y. Nishibayashi, *Organometallics* **2018**, *37*, 3086-3092.

[7] (a) S. Takaoka, A. Eizawa, S. Kusumoto, K. Nakajima, Y. Nishibayashi, K. Nozaki, *Organometallics* **2018**, *37*, 3001-3009; (b) X. Liu, B. Liu, Q. Liu, *Angew. Chem. Int. Ed.* **2020**, *n/a*; (c) M. Hernández-Juárez, J. López-Serrano, P. Lara, J. P. Morales-Cerón, M. Vaquero, E. Álvarez, V. Salazar, A. Suárez, *Chem. Eur. J.* **2015**, *21*, 7540-7555.

[8] (a) R. Arevalo, P. J. Chirik, *J. Am. Chem. Soc.* **2019**, *141*, 9106-9123; (b) G. A. Filonenko, M. J. B. Aguila, E. N. Schulpen, R. van Putten, J. Wiecko, C. Müller, L. Lefort, E. J. M. Hensen, E. A. Pidko, *J. Am. Chem. Soc.* **2015**, *137*, 7620-7623; (c) K. Tokmic, C. R. Markus, L. Zhu, A. R. Fout, *J. Am. Chem. Soc.* **2016**, *138*, 11907-11913; (d) A. Eizawa, K. Arashiba, H. Tanaka, S. Kuriyama, Y. Matsuo, K. Nakajima, K. Yoshizawa, Y. Nishibayashi, *Nature Communications* **2017**, *8*, 14874; (e) M. Darari, E. Domenichini, A. Francés-Monerris, C. Cebrián, K. Magra, M. Beley, M. Pastore, A. Monari, X. Assfeld, S. Haacke, P. C. Gros, *Dalton Trans.* **2019**, *48*, 10915-10926.

[9] (a) M. Raynal, C. S. J. Cazin, C. Vallée, H. Olivier-Bourbigou, P. Braunstein, *Chem. Commun.* **2008**, 3983-3985; (b) W. Zuo, P. Braunstein, *Organometallics* **2012**, *31*, 2606-2615; (c) N. Darmawan, C.-H. Yang, M. Mauro, M. Raynal, S. Heun, J. Pan, H. Buchholz, P. Braunstein, L. De Cola, *Inorg. Chem.* **2013**, *52*, 10756-10765; (d) M. Jagenbrein, A. A. Danopoulos, P. Braunstein, *J. Organomet. Chem.* **2015**, *775*, 169-172; (e) E. B. Bauer, G. T. S. Andavan, T. K. Hollis, R. J. Rubio, J. Cho, G. R. Kuchenbeiser, T. R. Helgert, C. S. Letko, F. S. Tham, *Org. Lett.* **2008**, *10*, 1175-1178.

[10] (a) A. R. Chianese, A. Mo, N. L. Lampland, R. L. Swartz, P. T. Bremer, *Organometallics* **2010**, *29*, 3019-3026; (b) A. R. Chianese, S. E. Shaner, J. A. Tendler, D. M. Pudalov, D. Y. Shopov, D. Kim, S. L. Rogers, A. Mo, *Organometallics* **2012**, *31*, 7359-7367; (c) A. R. Chianese, M. J. Drance, K. H. Jensen, S. P. McCollom, N. Yusufova, S. E. Shaner, D. Y. Shopov, J. A. Tendler, *Organometallics* **2014**, *33*, 457-464; (d) S. M. M. Knapp, S. E. Shaner, D. Kim, D. Y. Shopov, J. A. Tendler, D. M. Pudalov, A. R. Chianese, *Organometallics* **2014**, *33*, 473-484.

[11] (a) M. Raynal, C. S. J. Cazin, C. Vallée, H. Olivier-Bourbigou, P. Braunstein, *Organometallics* **2009**, *28*, 2460-2470; (b) M. Raynal, R. Pattacini, C. S. J. Cazin, C. Vallée, H. Olivier-Bourbigou, P. Braunstein, *Organometallics* **2009**, *28*, 4028-4047.

[12] K. M. Schultz, K. I. Goldberg, D. G. Gusev, D. M. Heinekey, *Organometallics* **2011**, *30*, 1429-1437.

[13] A. A. Danopoulos, D. Pugh, J. A. Wright, *Angew. Chem. Int. Ed.* **2008**, *47*, 9765-9767.

[14] M. R. Gyton, B. Leforestier, A. B. Chaplin, *Organometallics* **2018**, *37*, 3963-3971.

[15] (a) L.-H. Chung, K.-S. Cho, J. England, S.-C. Chan, K. Wieghardt, C.-Y. Wong, *Inorg. Chem.* **2013**, *52*, 9885-9896; (b) Y. Arikawa, T. Nakamura, S. Ogushi, K. Eguchi, K. Umakoshi, *Dalton Trans.* **2015**, *44*, 5303-5305; (c) C. M. Boudreaux, N. P. Liyanage, H. Shirley, S. Siek, D. L. Gerlach, F. Qu, J. H. Delcamp, E. T. Papish, *Chem. Commun.* **2017**, *53*, 11217-11220; (d) S. Das, R. R. Rodrigues, R. W. Lamb, F. Qu, E. Reinheimer, C. M. Boudreaux, C. E. Webster, J. H. Delcamp, E. T. Papish, *Inorg. Chem.* **2019**, *58*, 8012-8020.

[16] (a) E. Ben-Ari, R. Cohen, M. Gandelman, L. J. W. Shimon, J. M. L. Martin, D. Milstein, *Organometallics* **2006**, *25*, 3190-3210; (b) S. M. Kloek, D. M. Heinekey, K. I. Goldberg, *Organometallics* **2006**, *25*, 3007-3011.

[17] A. A. Danopoulos, D. Pugh, H. Smith, J. Saßmannshausen, *Chem. Eur. J.* **2009**, *15*, 5491-5502.

[18] J. Saßmannshausen, A. A. Danopoulos, P. Braunstein, *Unpublished results*.

[19] (a) R. Pattacini, S. Jie, P. Braunstein, *Chem. Commun.* **2009**, 890-892; (b) A. G. Algarra, P. Braunstein, S. A. Macgregor, *Dalton Trans.* **2013**, *42*, 4208-4217.

[20] J. A. Wright, A. A. Danopoulos, W. B. Motherwell, R. J. Carroll, S. Ellwood, J. Saßmannshausen, *Eur. J. Inorg. Chem.* **2006**, *2006*, 4857-4865.

[21] (a) D. Sieh, J. Schöffel, P. Burger, *Dalton Trans.* **2011**, *40*, 9512-9524; (b) I. Mena, E. A. Jaseer, M. A. Casado, P. García-Orduña, F. J. Lahoz, L. A. Oro, *Chem. Eur. J.* **2013**, *19*, 5665-5675.

[22] L. Vaquer, P. Miró, X. Sala, F. Bozoglian, E. Masllorens, J. Benet-Buchholz, X. Fontrodona, T. Parella, I. Romero, A. Roglans, M. Rodríguez, C. Bo, A. Llobet, *ChemPlusChem* **2013**, *78*, 235-243.

[23] E. Masllorens, M. Rodríguez, I. Romero, A. Roglans, T. Parella, J. Benet-Buchholz, M. Poyatos, A. Llobet, *J. Am. Chem. Soc.* **2006**, *128*, 5306-5307.

[24] C. G. Leong, O. M. Akotsi, M. J. Ferguson, S. H. Bergens, *Chem. Commun.* **2003**, 750-751.

[25] O. M. Akotsi, K. Metera, R. D. Reid, R. McDonald, S. H. Bergens, *Chirality* **2000**, *12*, 514-522.

[26] Y. Zhang, H. Fang, W. Yao, X. Leng, Z. Huang, *Organometallics* **2016**, *35*, 181-188.

[27] A. A. Danopoulos, S. Winston, W. B. Motherwell, *Chem. Commun.* **2002**, 1376-1377.

[28] (a) S. Grimme, *J. Comput. Chem.* **2006**, *27*, 1787-1799; (b) S. Grimme, J. Antony, S. Ehrlich, H. Krieg, *J. Chem. Phys.* **2010**, *132*, 154104; (c) U. Ryde, R. A. Mata, S. Grimme, *Dalton Trans.* **2011**, *40*, 11176-11183.

[29] S. Barnett, D. Allan, M. Gutmann, J. K. Cockcroft, V. H. Mai, A. E. Aliev, J. Saßmannshausen, *Inorg. Chim. Acta* **2019**, *488*, 292-298.

[30] J. Contreras-García, E. R. Johnson, S. Keinan, R. Chaudret, J.-P. Piquemal, D. N. Beratan, W. Yang, *J. Chem. Theory Comput.* **2011**, *7*, 625-632.

[31] D. Pugh, A. Boyle, A. A. Danopoulos, *Dalton Trans.* **2008**, 1087-1094.

[32] M. Brookhart, B. Grant, A. F. Volpe, *Organometallics* **1992**, *11*, 3920-3922.

[33] M. J. Frisch, G. W. Trucks, H. B. Schlegel, G. E. Scuseria, M. A. Robb, J. R. Cheeseman, G. Scalmani, V. Barone, B. Mennucci, G. A. Petersson, H. Nakatsuji, M. Caricato, X. Li, H. P. Hratchian, A. F. Izmaylov, J. Bloino, G. Zheng, J. L. Sonnenberg, M. Hada, M. Ehara, K. Toyota, R. Fukuda, J. Hasegawa, M. Ishida, T. Nakajima, Y. Honda, O. Kitao, H. Nakai, T. Vreven, J. J. A. Montgomery, J. E. Peralta, F. Ogliaro, M. Bearpark, J. J. Heyd, E. Brothers, K. N. Kudin, V. N. Staroverov, T. Keith, R. Kobayashi, J. Normand, K. Raghavachari, A. Rendell, J. C. Burant, S. S. Iyengar, J. Tomasi, M. Cossi, N. Rega, J. M. Millam, M. Klene, J. E. Knox, J. B. Cross, V. Bakken, C. Adamo, J. Jaramillo, R. Gomperts, R. E. Stratmann, O. Yazyev, A. J. Austin, R. Cammi, C. Pomelli, J. W. Ochterski, R. L. Martin, K. Morokuma, V. G. Zakrzewski, G. A. Voth, P. Salvador, J. J. Dannenberg, S. Dapprich, A. D. Daniels, O. Farkas, J. B. Foresman, J. V. Ortiz, J. Cioslowski, D. J. Fox., Gaussian, Inc., Wallingford CT, **2010**.

[34] (a) J. P. Perdew, K. Burke, M. Ernzerhof, *Phys. Rev. Lett.* **1996**, *77*, 3865 LP - 3868; (b) V. Vetere, C. Adamo, P. Maldivi, *Chem. Phys. Lett.* **2000**, *325*, 99-105.

[35] (a) W. J. Hehre, R. Ditchfield, J. A. Pople, *J. Chem. Phys.* **1972**, *56*, 2257 - 2261; (b) P. C. Hariharan, J. A. Pople, *Theor. Chim. Acta* **1973**, *28*, 213 - 222.

[36] M. Bühl, C. Reimann, D. A. Pantazis, T. Bredow, F. Neese, *J. Chem. Theory Comput.* **2008**, *4*, 1449-1459.

[37] D. A. Pantazis, X.-Y. Chen, C. R. Landis, F. Neese, *J. Chem. Theory Comput.* **2008**, *4*, 908-919.

[38] (a) D. Feller, *J. Comp. Chem.* **1996**, *17*, 1571-1586; (b) K. L. Schuchardt, B. T. Didier, T. Elsethagen, L. Sun, V. Gurumoorthi, J. Chase, J. Li, T. L. Windus, *J. Chem. Inf. Model.* **2007**, *47*, 1045-1052; (c) B. P. Pritchard, D. Altarawy, B. Didier, T. D. Gibsom, T. L. Windus, *J. Chem. Inf. Model.* **2019**, *59*, 4814-4820.

[39] R. F. W. Bader, *Atoms in Molecules: A Quantum Theory*, Clarendon Press, Oxford, UK, **1990**.

[40] (a) F. Biegler-König, J. Schönbohm, D. Bayles, *J. Comp. Chem.* **2001**, *22*, 545-559; (b) F. Biegler-König, J. Schönbohm, *J. Comput. Chem.* **2002**, *23*, 1489-1494.

[41] (a) E. D. Glendening, J. K. Badenhoop, A. E. Reed, J. E. Carpenter, J. A. Bohmann, C. M. Morales, P. Karafiloglou, C. R. Landis, F. Weinhold, Theoretical Chemistry Institute, University of Wisconsin, Madison, WI, **2018**; (b) E. D. Glendening, C. R. Landis, F. Weinhold, *J. Comput. Chem.* **2019**, *40*, 2234-2241.

[42] Jmol: an open-source Java viewer for chemical structures in 3D. http://www.jmol.org/

Entry for the Table of Contents

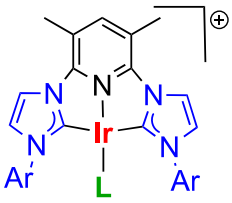

✓ Non-Covalent Interactions (L = Py)
✓ Oxidative-Addition Reactions
✓ Activation of CH_2Cl_2
✓ Comparisons with Ru^{II} Analogues

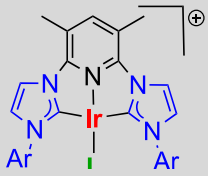

✓ Non-Covalent Interactions (L = Py)
✓ Oxidative-Addition Reactions
✓ Activation of CH_2Cl_2
✓ Comparisons with Ru^{II} Analogues

Synthesis, reactivity, structures and bonding analyses of Ir^{I} pincer-type complexes are reported. Specific geometrical distortions away from regular square-planar are discussed in the context of NCI. Analogous Ru^{II} complexes are also presented.